

Rosseland international team

WaLSA: Waves in the Lower Solar Atmosphere at high resolution

August 12-16, 2019, Rosseland Center for Solar Physics (RoCS)

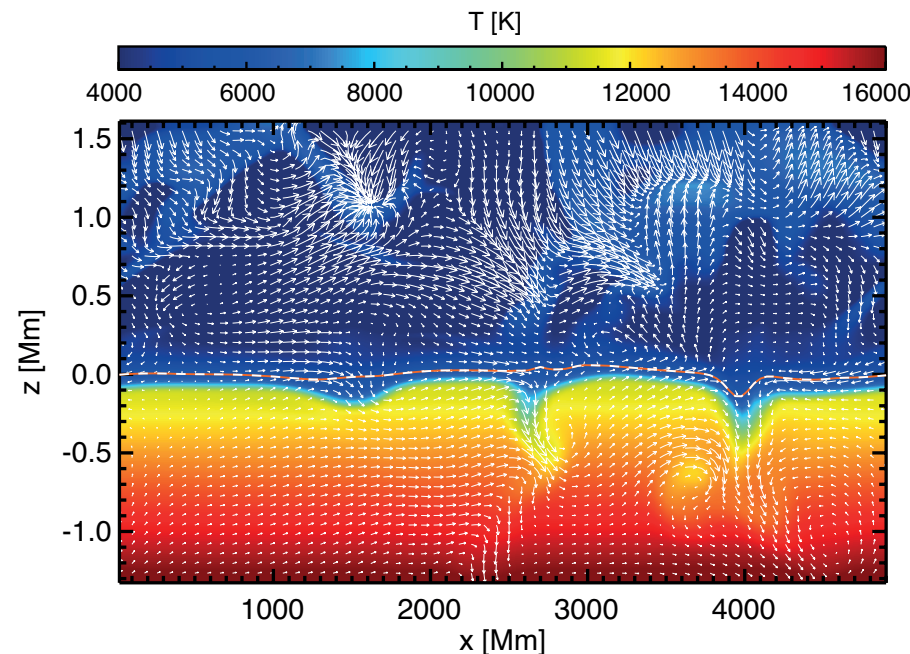
Waves and swirls

Oskar Steiner

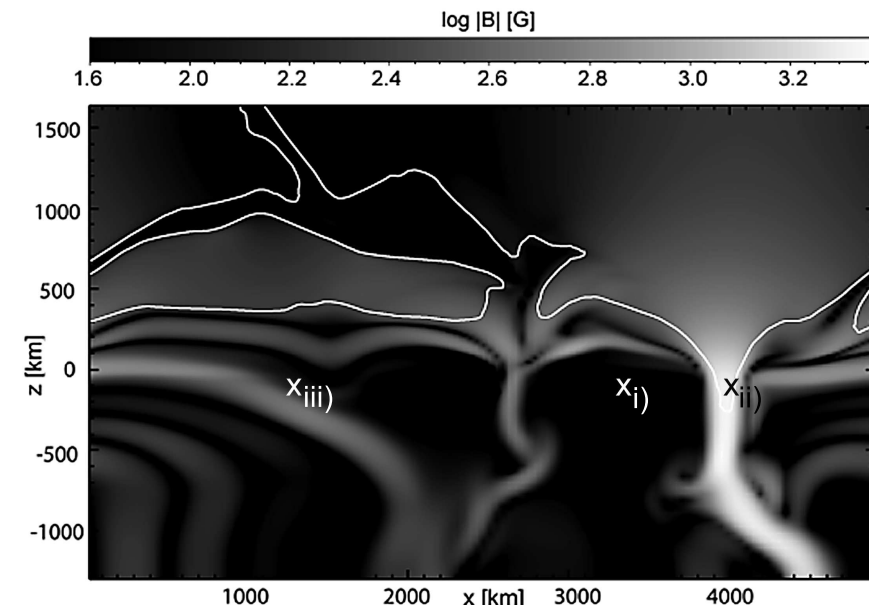
Leibniz-Institut für Sonnenphysik (KIS), Freiburg i.Br. and

Istituto Ricerche Solari Locarno (IRSOL), Locarno

§ 1 Wave conversion: a numerical experiment



Temperature (colors), velocity (arrows),
and optical depth $\tau_c = 1$ (dashed curve).

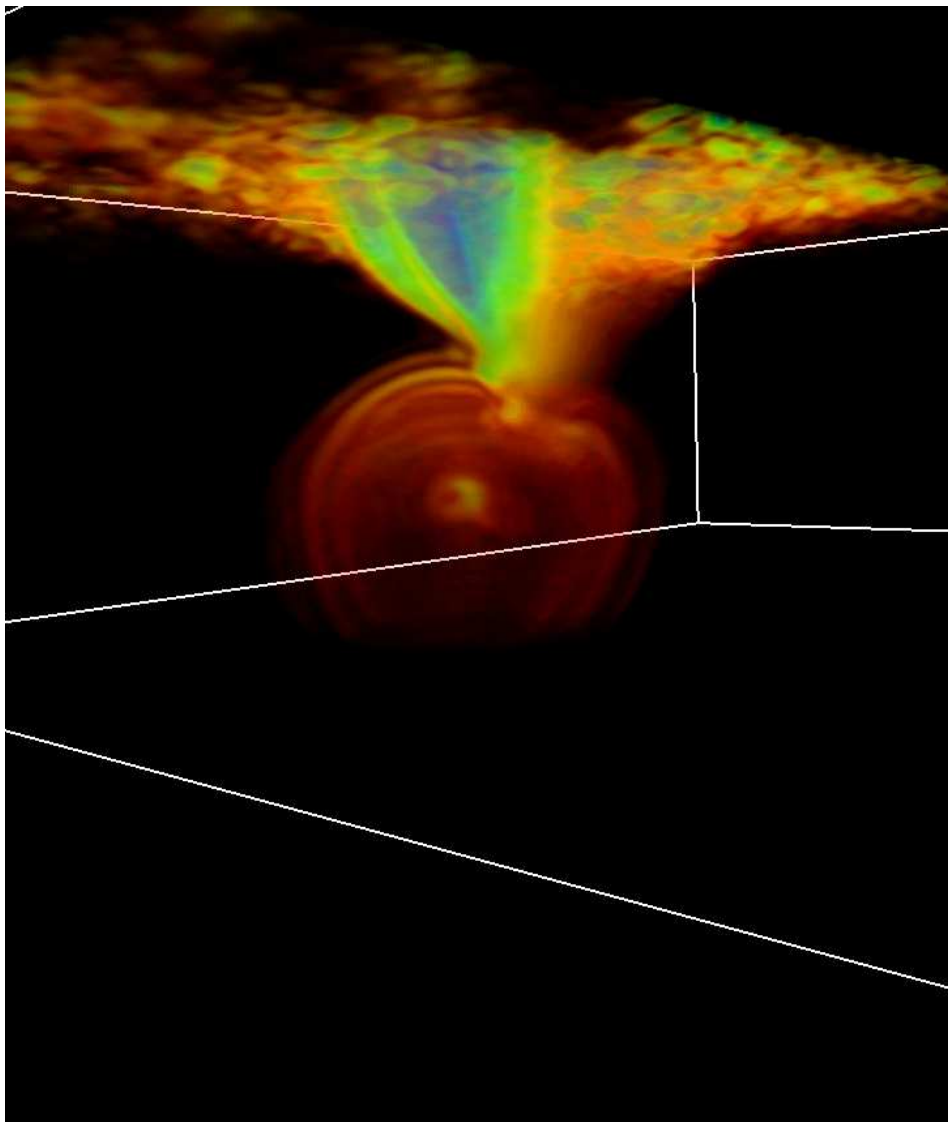


Magnetic field strength (gray scales), level
where $c_s = c_A$ (white contour), locations
of local wave excitation (crosses).

Movies of wave excitation at x_{i} , x_{ii} , x_{iii} , and along the lower boundary.

From Nutto et al., 2012 A&A 538, A79.

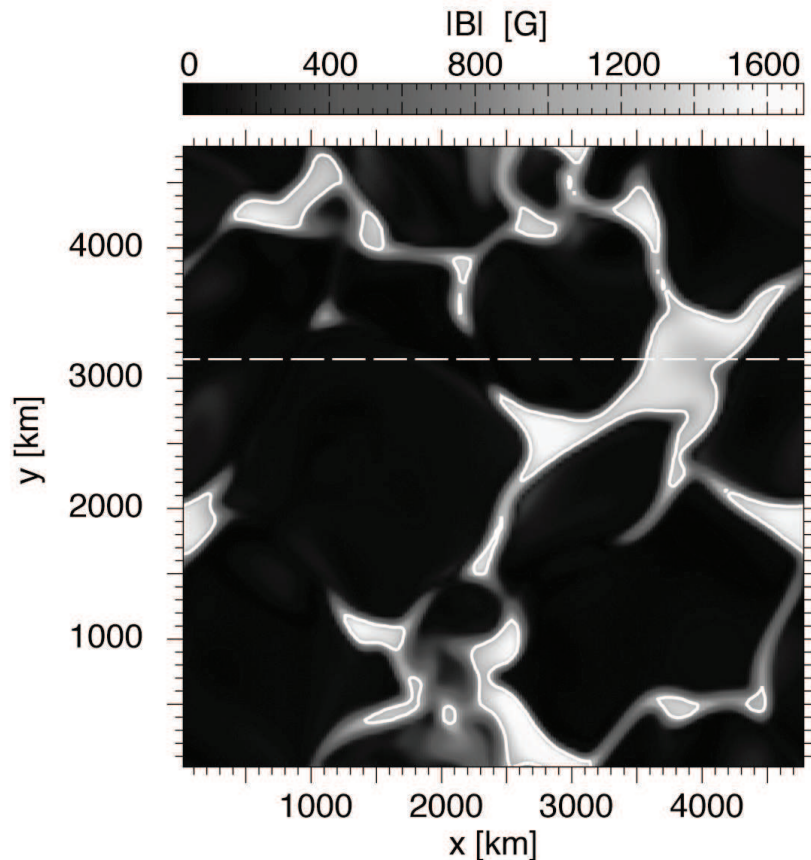
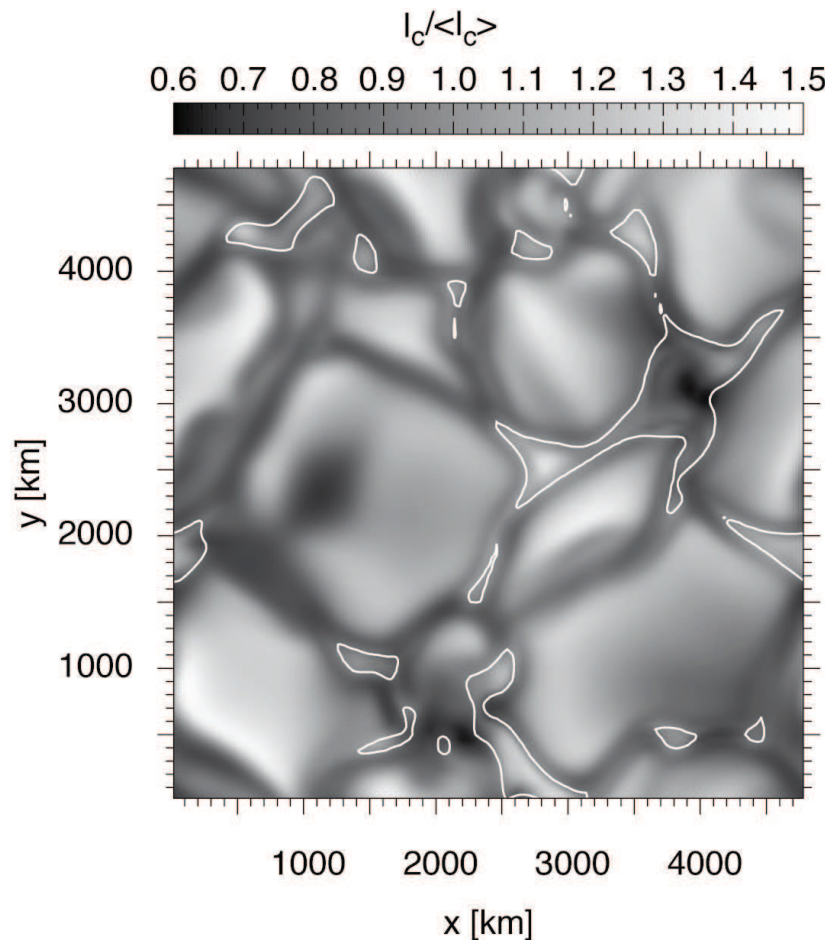
§ 1 Wave conversion: a numerical experiment (cont.)



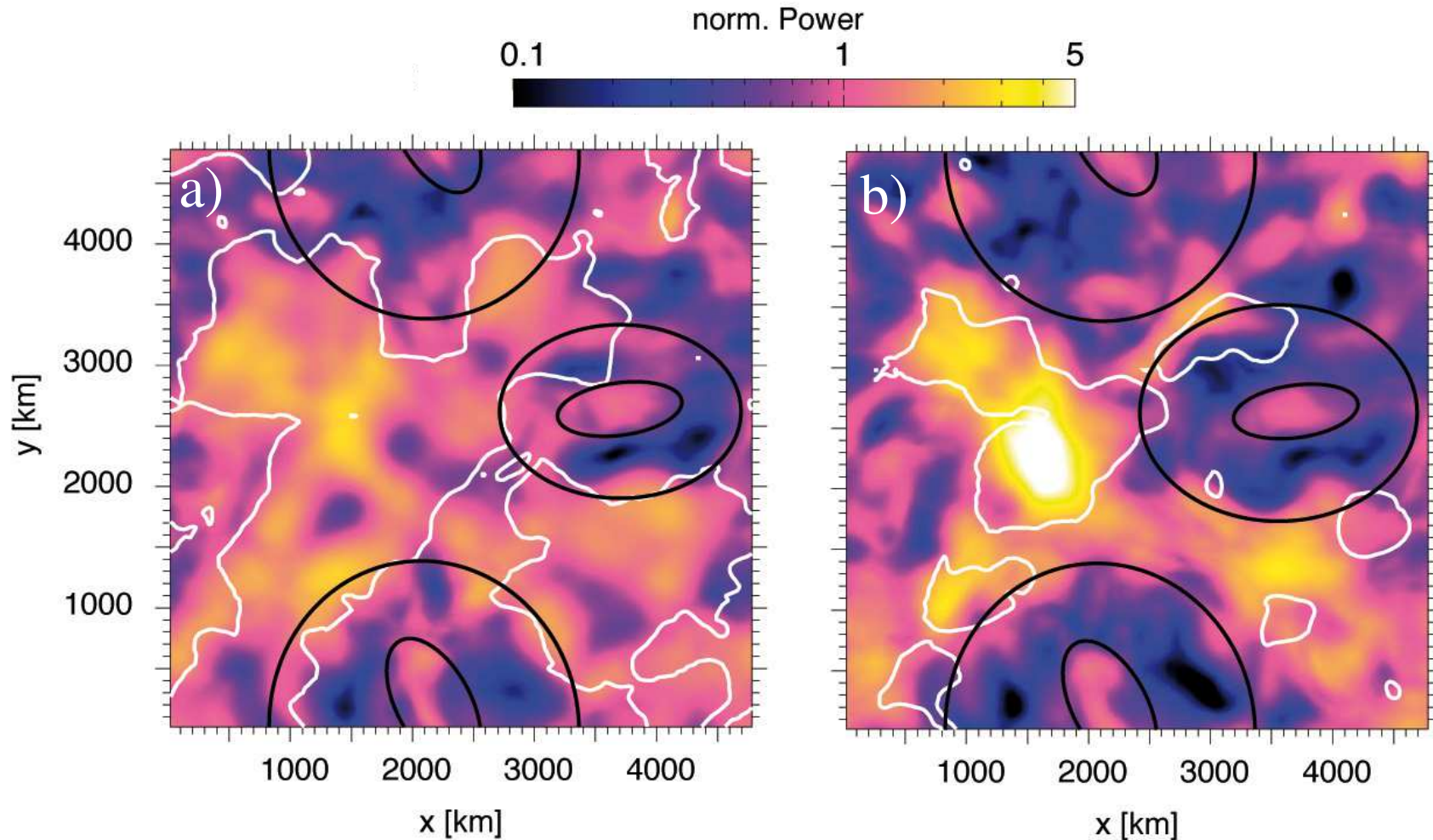
Time instant of a spherical, fast acoustic wave, initiated by a local pressure perturbation in the convection zone. When the wave encounters the low beta magnetic flux concentration in the photosphere, it partially converts into a fast magnetic mode, which shows the typical “fanning out” already encountered in the 2-D simulation. Colors show absolute velocity perturbation.

Courtesy *Christian Nutto, KIS*.

§ 1.1 Magnetic halos and shadows

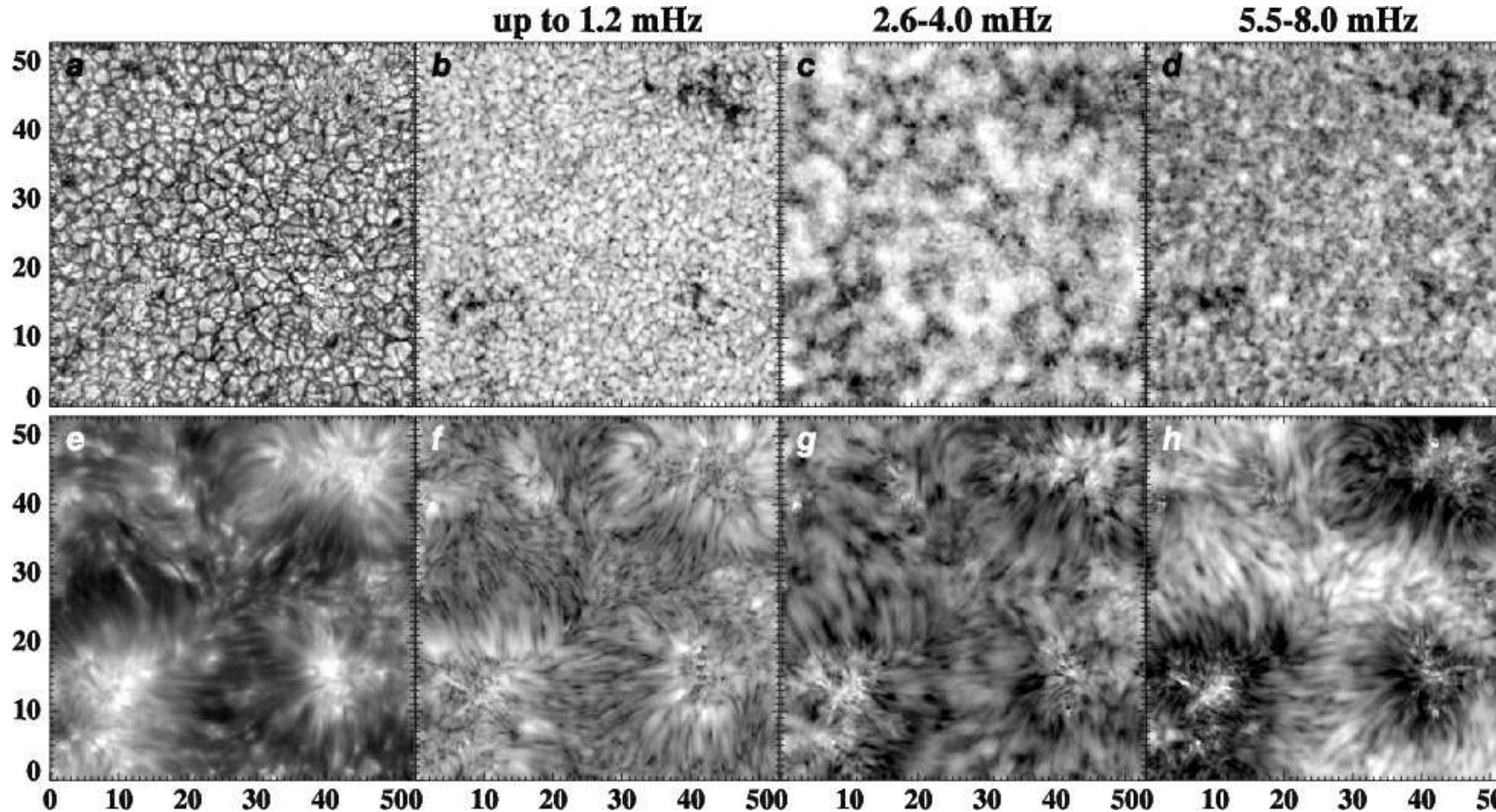


§ 1.1 Magnetic halos and shadows (cont.)



Power maps of the vertical velocity perturbations, δv_z , taken at a) $\tau_c = 8 \cdot 10^{-4}$ and b) $\tau_c = 6.7 \cdot 10^{-5}$. The *white contours* shows the equipartition level $c_s = c_A$. The *ellipses* mark regions where the *magnetic shadow* can be identified. Note suppression of power in the region between the large and the small ellipses. From Nutto et al. 2012.

§ 1.1 Magnetic halos and shadows (cont.)

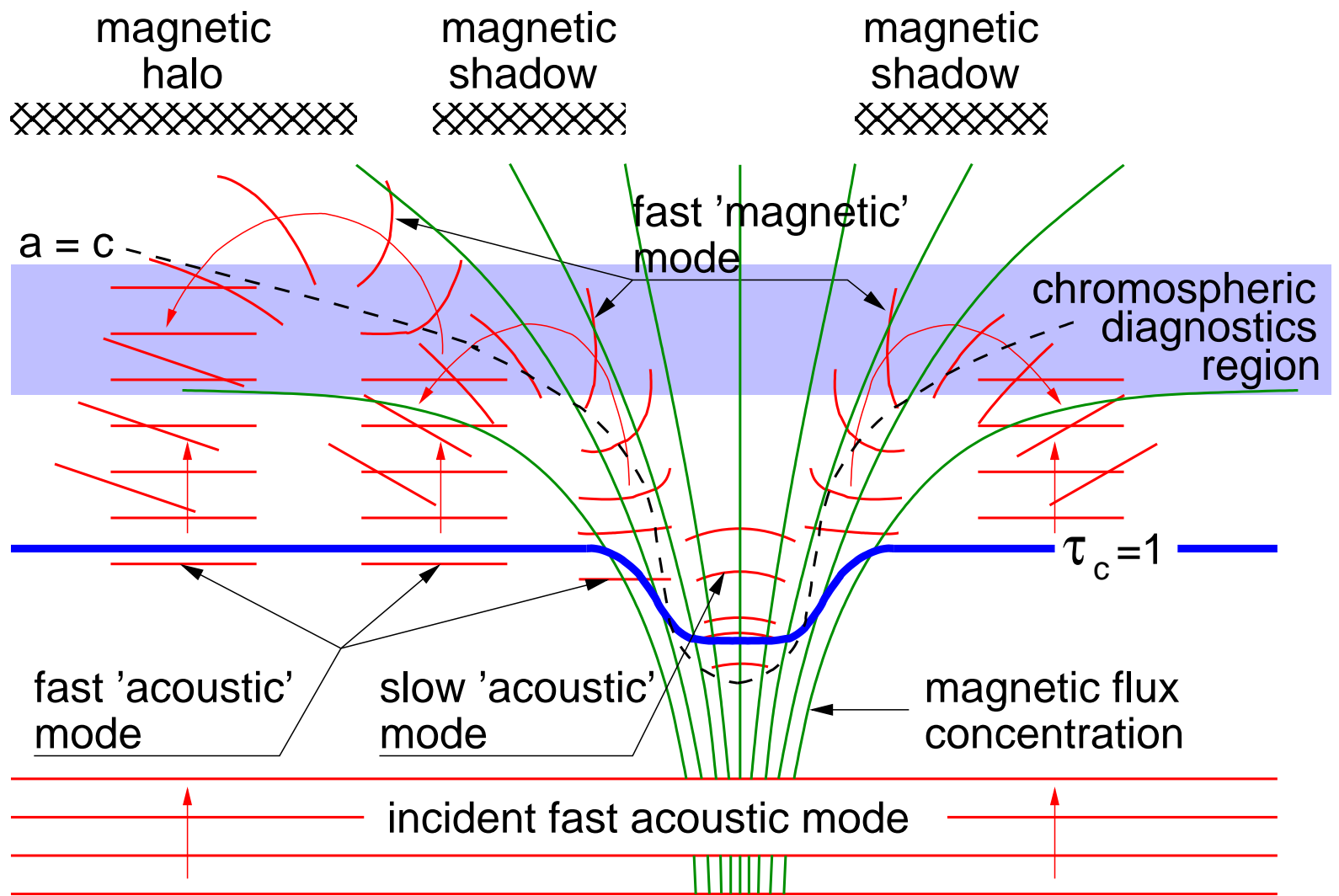


a) Broadband continuum at 710 nm. e) Line core intensity of Ca II 854.2 nm. b)–d) and f)–h)

Logarithm of the Fourier Doppler-velocity power averaged over the indicated range of frequencies of the photospheric line Fe I 709.0 nm (b)–d)) and the chromospheric line Ca II 854.2 nm (f)–h)).

From Vecchio, Cauzzi, Reardon et al. (2007), A&A 461, L1. obtained with IBIS at DST.

§ 1.1 Magnetic halos and shadows (cont.)

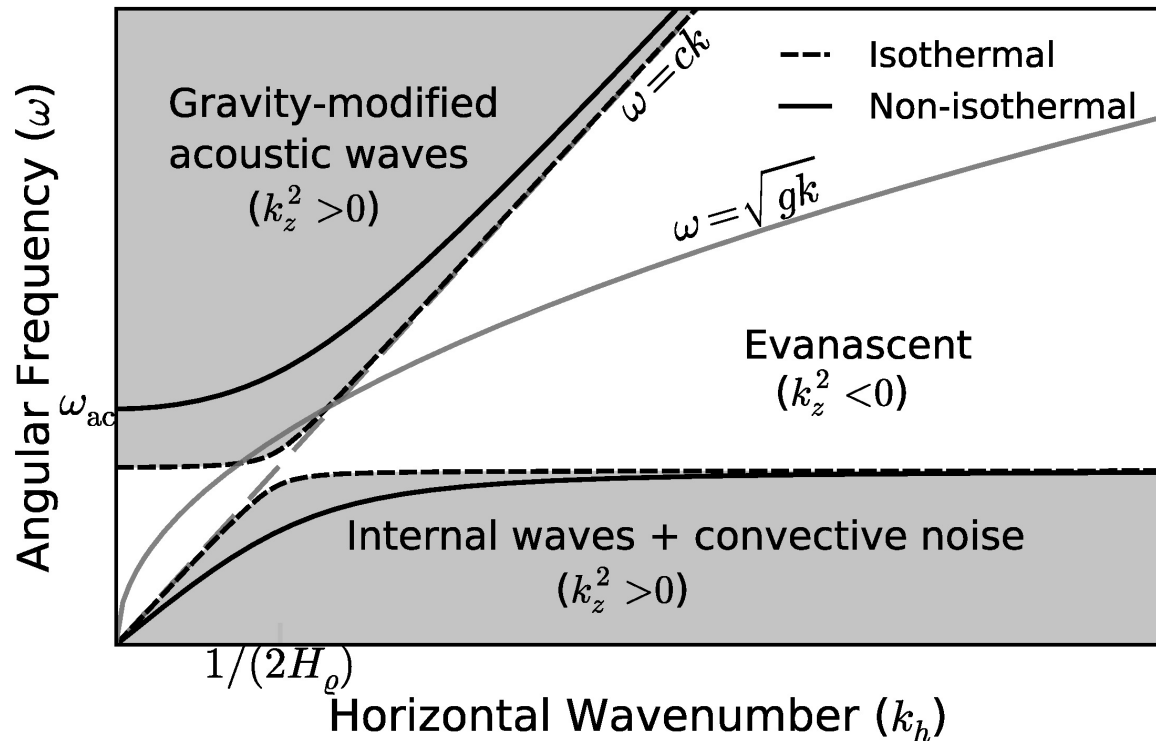


From Komm, De Moortel, Fan, Ilinidis & Steiner, 2015
Space Sci. Rev 196, 167-199.

Sketch of the three different magneto-acoustic modes that lead to the phenomenon of the magnetic shadow and the magnetic halo.

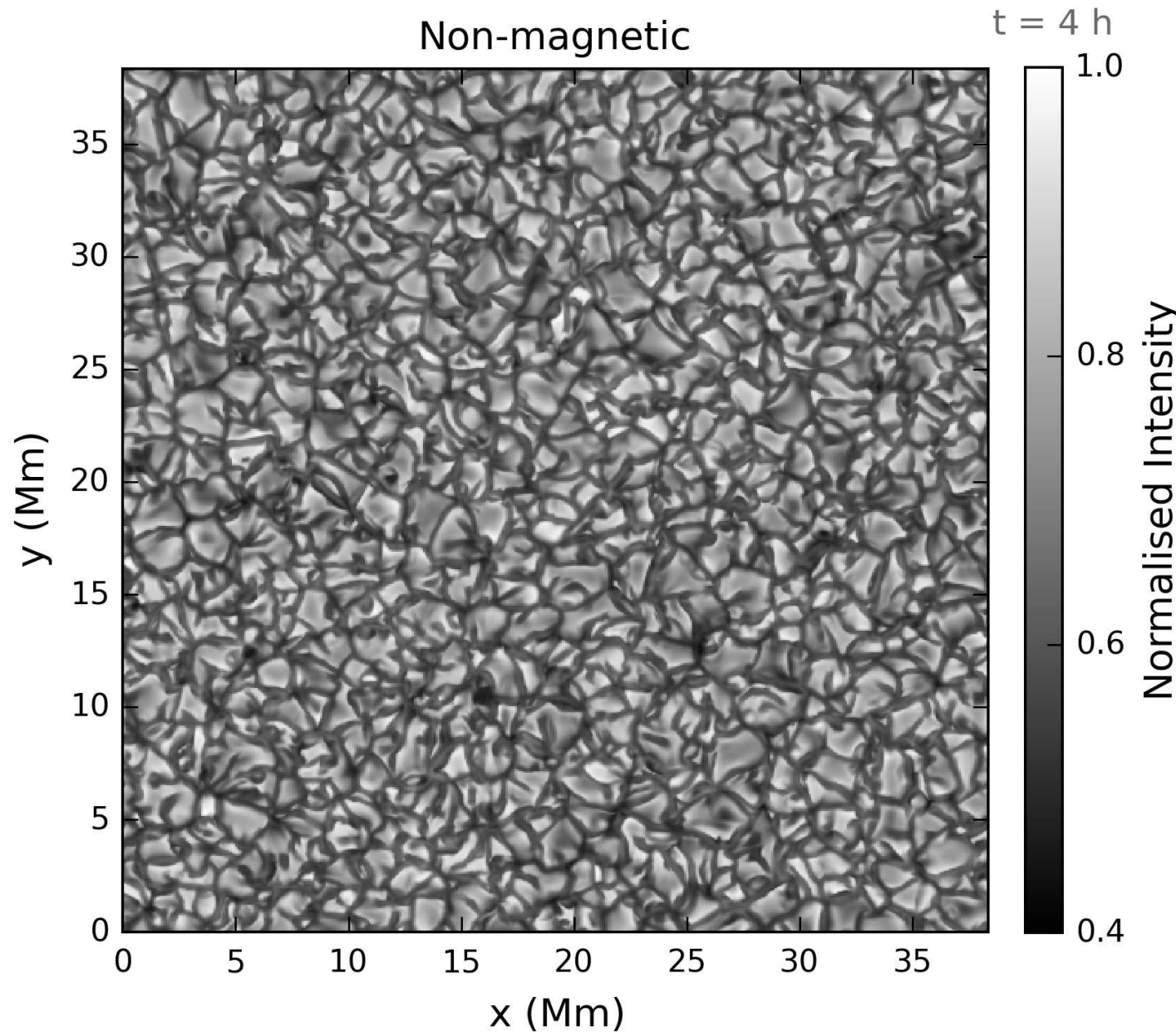
§ 2 Gravity waves

Gravity waves occur in the stable stratified (subadiabatic) part of the solar atmosphere, i.e., above the convection zone. Their restoring force is *buoyancy*. They are excited by *convective overshoot* into the photosphere.



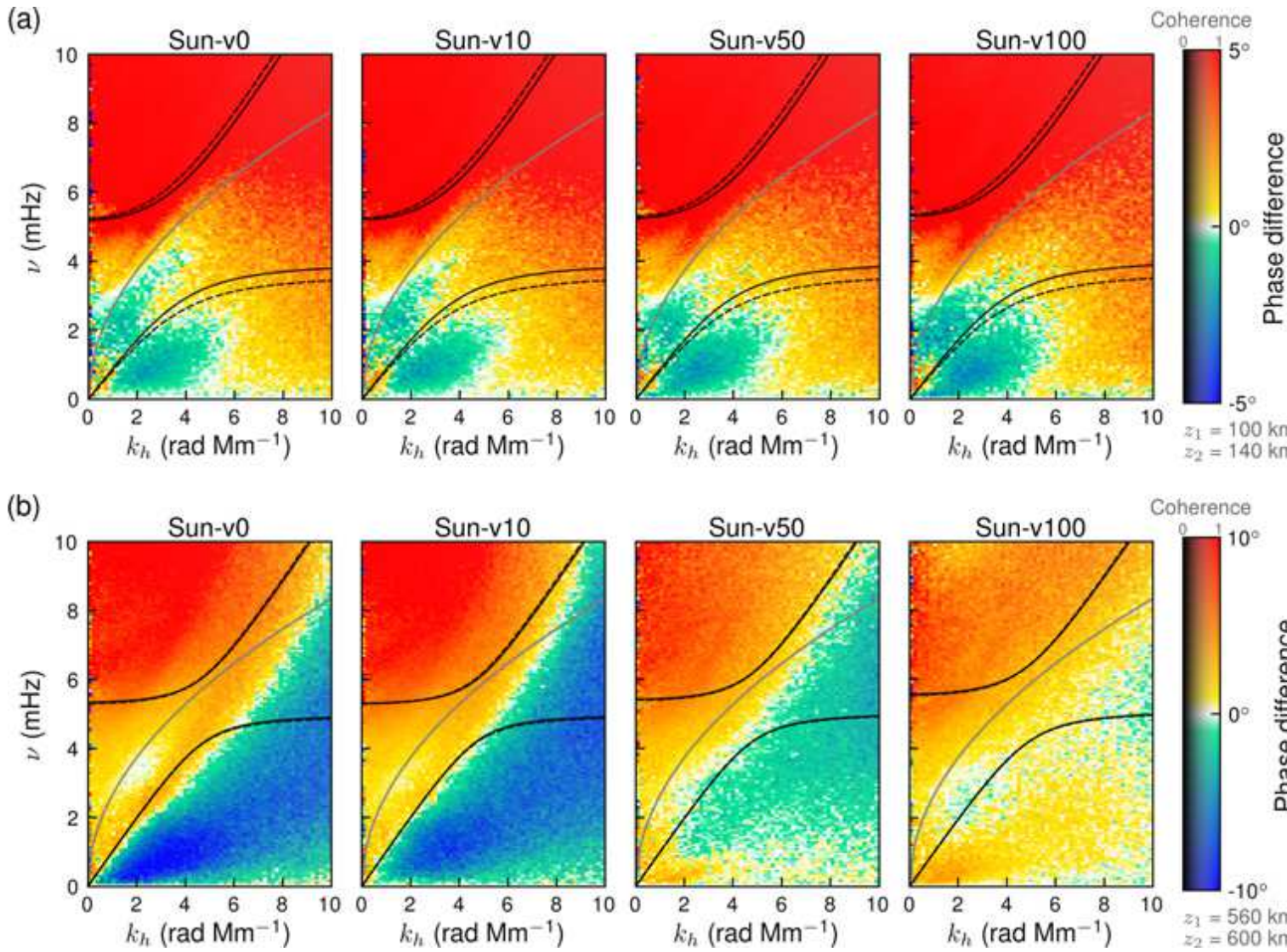
Schematic of the *diagnostic diagram* for a particular height in the atmosphere. $\omega_{ac} = c_s / (2H_p)$ is the acoustic cutoff period, N the Brunt-Väisälä frequency. Internal, or gravity waves have frequencies $\omega < N$.

§ 2 Gravity waves (cont.)



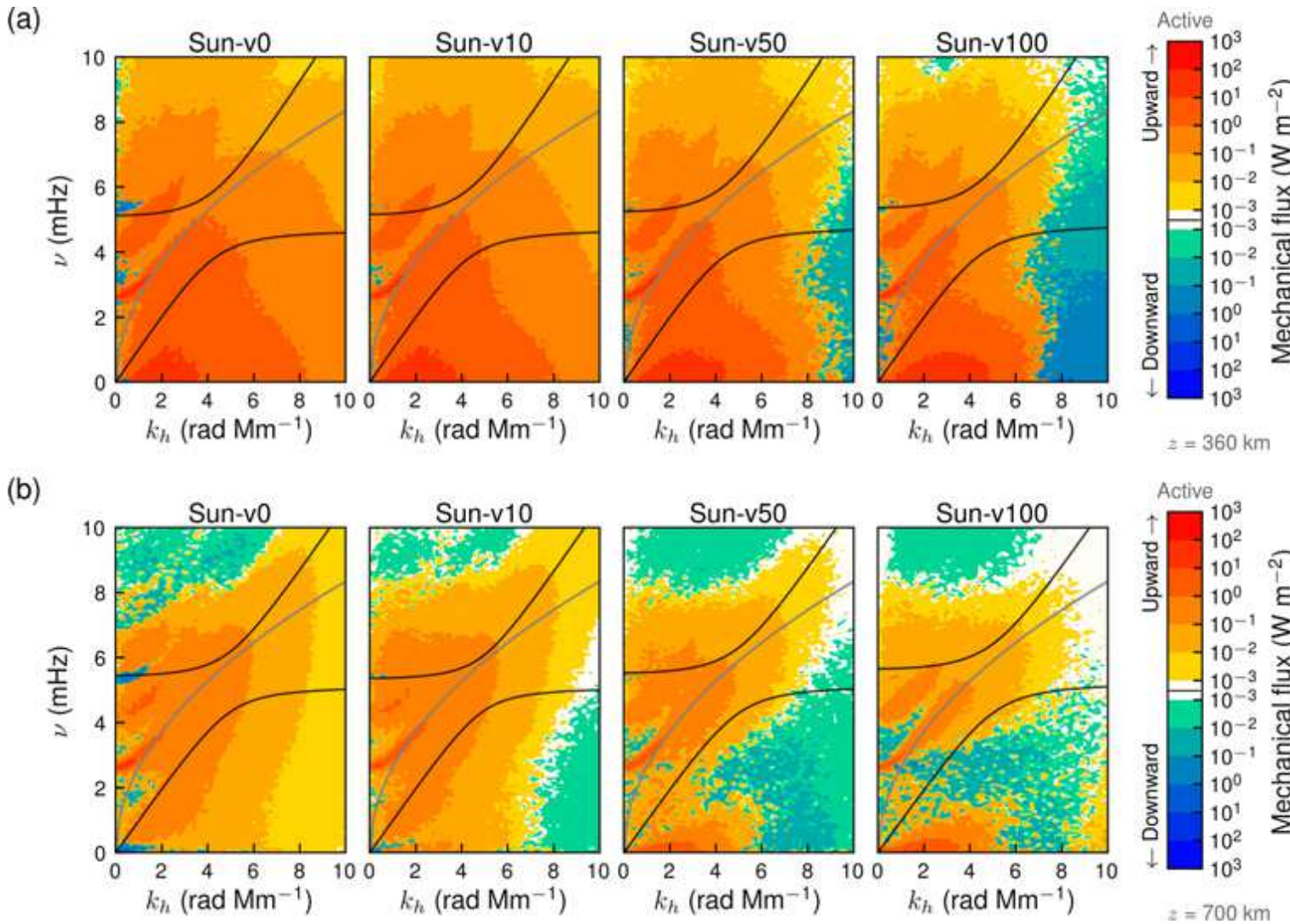
Simulation of *convective overshoot* into the stable stratified photosphere. The simulation domain is $38.4 \times 38.4 \times 2.8 \text{ Mm}^3$ and runs for 8 h physical time. From *Vigeesh et al., 2017*.

§ 2 Gravity waves (cont.)



Synthetic $v_z - v_z$ phase difference spectra between heights of a) $z = 100 \text{ km}$ and $z = 140 \text{ km}$, and b) $z = 560 \text{ km}$ and $z = 600 \text{ km}$, for the non-magnetic model (v0) and the magnetic models (v10, v50, v100). Note the absence of upwardly propagating gravity waves in the upper layers of the models v50 and v100. From Vigeesh et al., 2019.

§ 2 Gravity waves (cont.)



Vertical mechanical flux spectrum at a height of a) $z = 360 \text{ km}$ and b) $z = 700 \text{ km}$ for the nonmagnetic model (v0) and the three magnetic models (v10, v50, v100). Note downward propagating mechanical flux in the gravity wave regime in the upper layers of models v50 and v100. From Vigeesh et al., 2019.

$$F_M(\mathbf{k}, \omega) = \frac{1}{2} \mathcal{C}_{p',v}(\mathbf{k}, \omega) = \frac{1}{2} \text{Re}\{p'(\mathbf{k}, \omega) \overline{v(\mathbf{k}, \omega)}\}$$

§ 2 Gravity waves (cont.)

Possible explanations for the absence of propagating internal waves in the upper atmosphere of the magnetic simulation are:

- *Mode conversion* of the internal wave *to Alfvénic waves* (unlikely in the present case because to the predominant vertically directed magnetic field);
- Mode coupling to magneto-acoustic waves and *reflection* back into the atmosphere as described by Newington & Cally (2010, 2011).
- Non-linear interaction of internal waves with shear flows, leading to the *breaking of internal waves into turbulence*. (shear flows are provided by swirling motion in the upper atmosphere induced by the mangetic field)

§ 3 Swirls in the solar atmosphere

Vorticity $\omega = \nabla \times \mathbf{v}$ is the standard quantity to study vortical flows in fluid dynamics. However, vorticity does not distinguish a shear flow from an actual vortex. To isolate vortices, Zhou et al. (1999) suggest to use the *velocity gradient tensor*

$$D_{ij} = \partial_j v_i \iff D = \begin{bmatrix} \partial_x v_x & \partial_y v_x & \partial_z v_x \\ \partial_x v_y & \partial_y v_y & \partial_z v_y \\ \partial_x v_z & \partial_y v_z & \partial_z v_z \end{bmatrix}.$$

ω corresponds to the antisymmetrized version of D ; $D - D^T$.

§ 3 Swirls in the solar atmosphere (cont.)

It can be shown that D can be decomposed in the following form:

$$D = (\mathbf{u}_r, \mathbf{u}_{cr}, \mathbf{u}_{ci}) \begin{bmatrix} \lambda_r & 0 & 0 \\ 0 & \lambda_{cr} & \lambda_{ci} \\ 0 & -\lambda_{ci} & \lambda_{cr} \end{bmatrix} (\mathbf{u}_r, \mathbf{u}_{cr}, \mathbf{u}_{ci})^{-1}$$

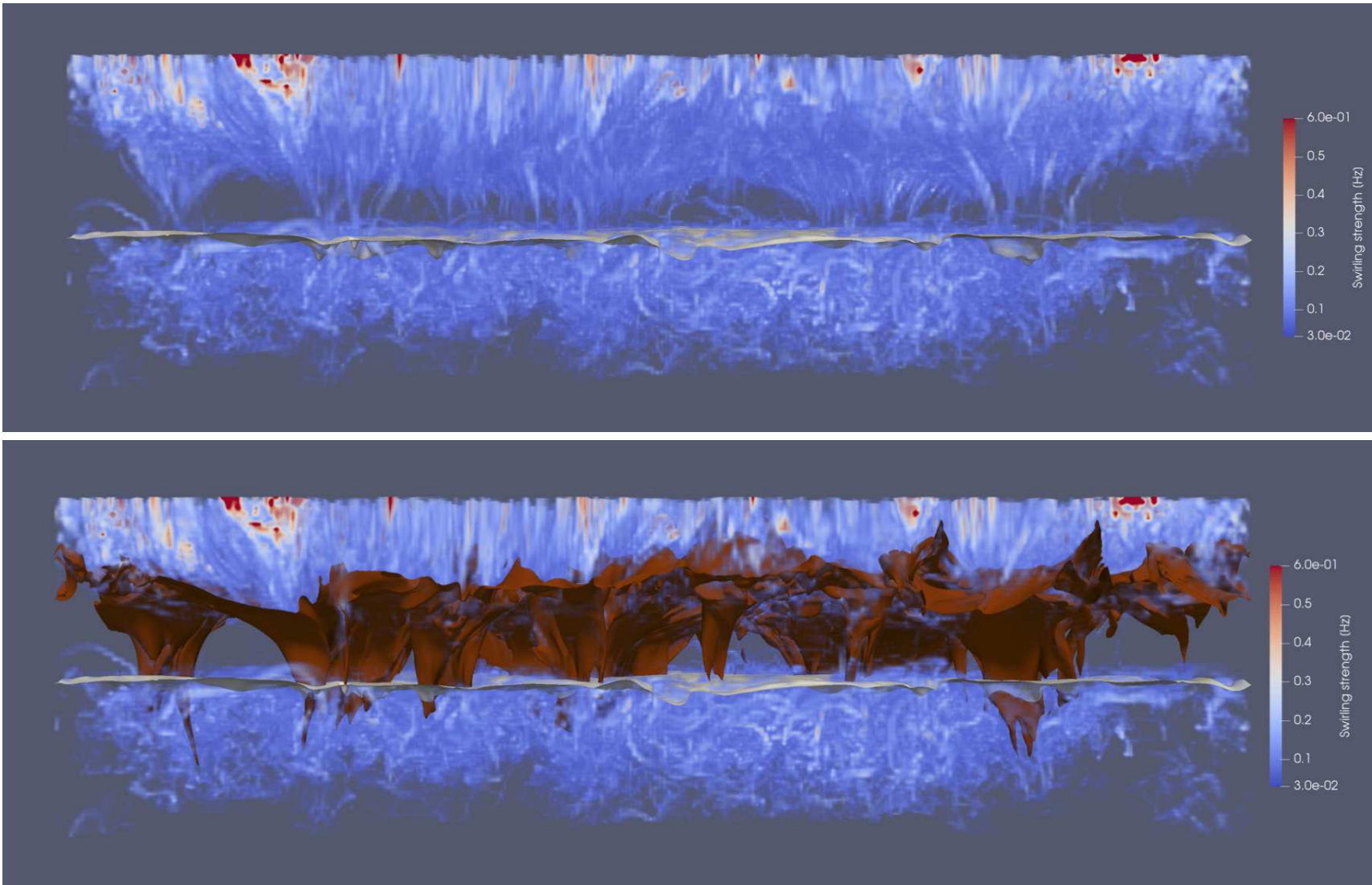
$$= (\mathbf{u}_r, \mathbf{u}_+, \mathbf{u}_-) \begin{bmatrix} \lambda_r & 0 & 0 \\ 0 & \lambda_+ & 0 \\ 0 & 0 & \lambda_- \end{bmatrix} (\mathbf{u}_r, \mathbf{u}_+, \mathbf{u}_-)^{-1},$$

where $\mathbf{u}_+ = \frac{1}{\sqrt{2}}(\mathbf{u}_{cr} + i\mathbf{u}_{ci})$, $\mathbf{u}_- = \frac{1}{\sqrt{2}}(\mathbf{u}_{cr} - i\mathbf{u}_{ci})$,

and $\lambda_+ = \frac{1}{\sqrt{2}}(\lambda_{cr} + i\lambda_{ci})$, $\lambda_- = \frac{1}{\sqrt{2}}(\lambda_{cr} - i\lambda_{ci})$.

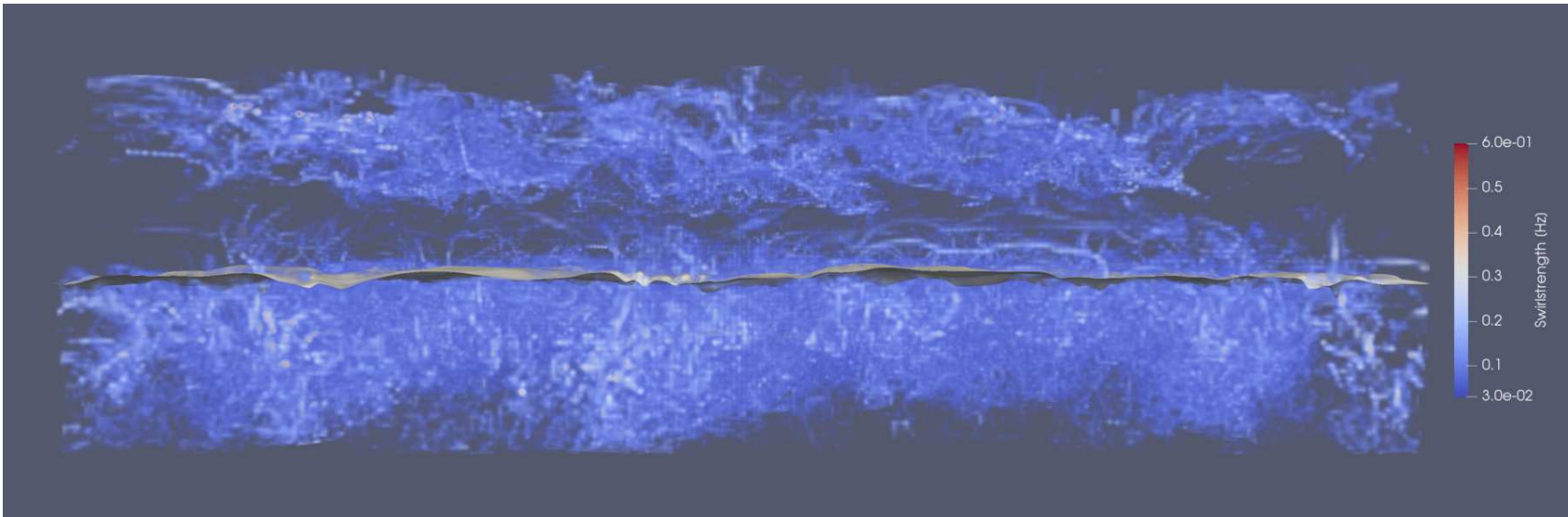
$\sqrt{2}\lambda_{ci} \equiv \lambda$ measures the *swirling strength* of the rotative flow, where $4\pi/\lambda = T$ is the period of the rotation and \mathbf{u}_r is the rotation axis.

§ 3 Swirls in the solar atmosphere (cont.)



Swirling strength with iso-surface $\tau = 1$ (white) and iso-surface $\beta = 1$ (red).

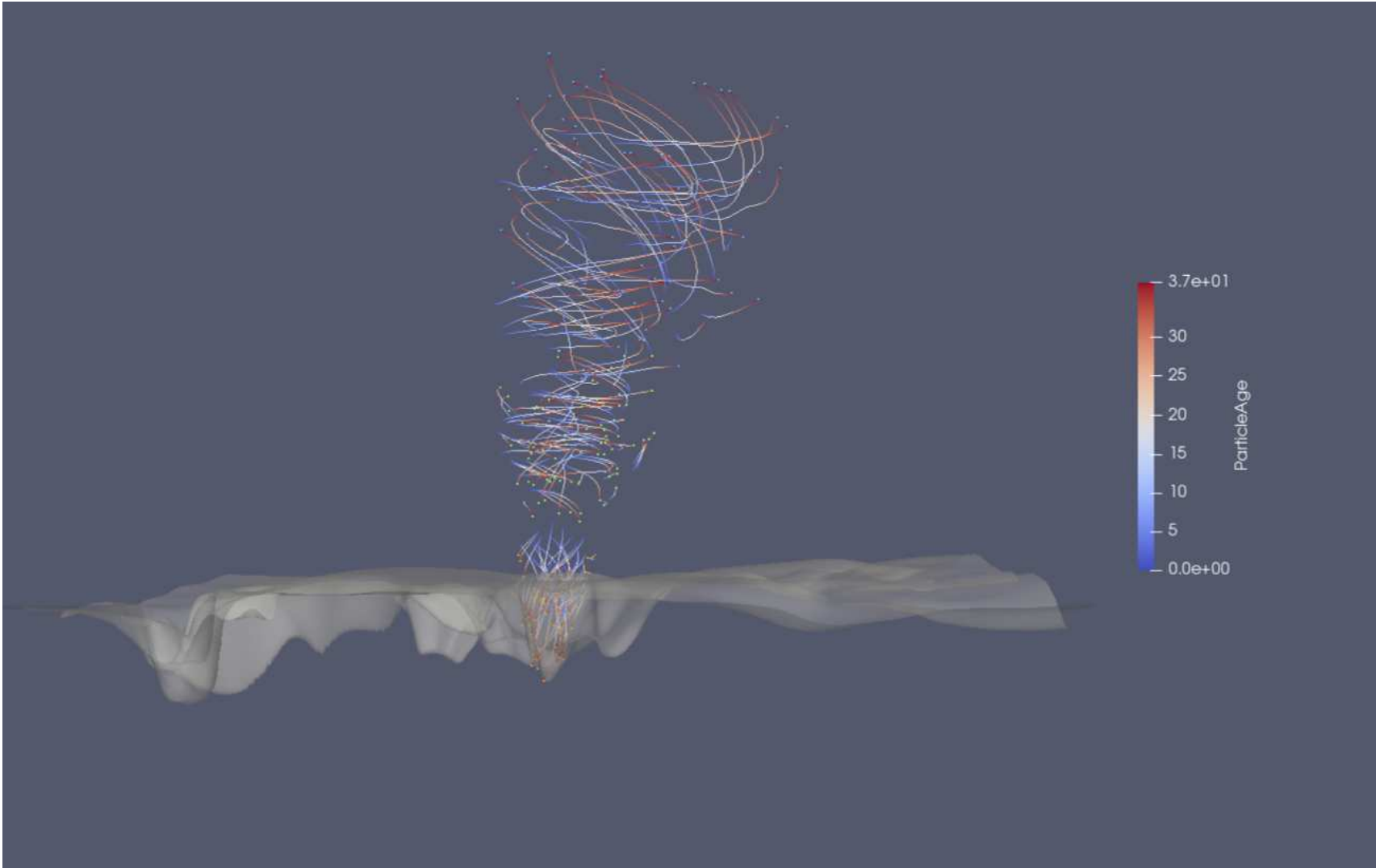
§ 3 Swirls in the solar atmosphere (cont.)



Swirling strength of a magnetic field-free simulation for comparison.

From *Bossart, A., 2018, IRSOL internal report.*

§ 3 Swirls in the solar atmosphere (cont.)

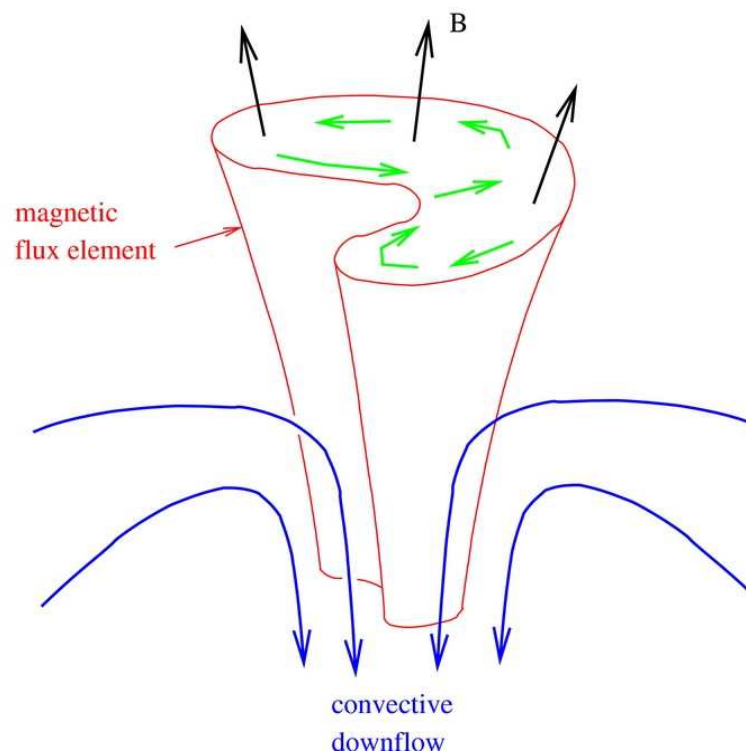
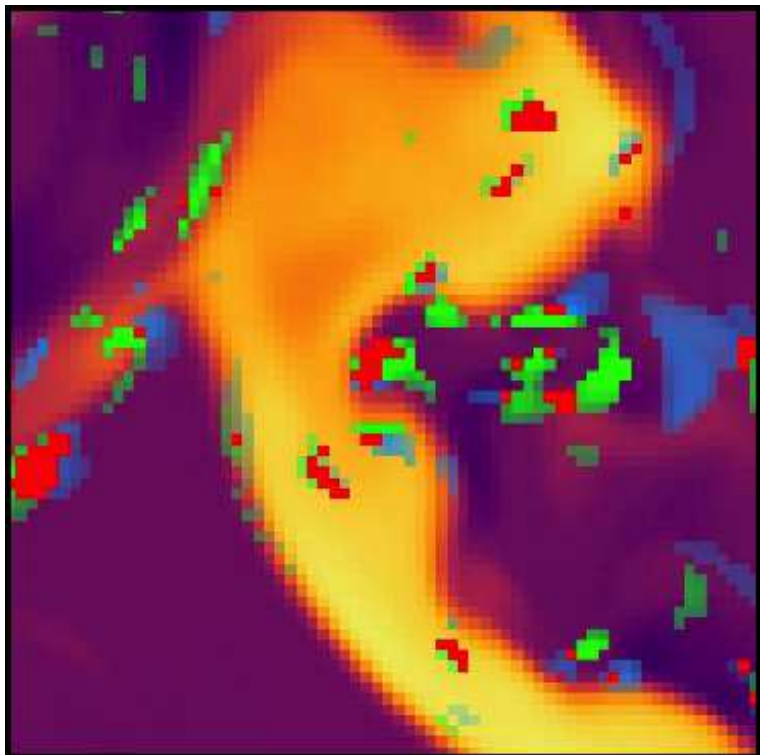


Particle tracks. Color range indicates time, starting with blue and turning red with age.

From *Bossart, A., 2018, IRSOL internal report.*

§ 3 Swirls in the solar atmosphere (cont.)

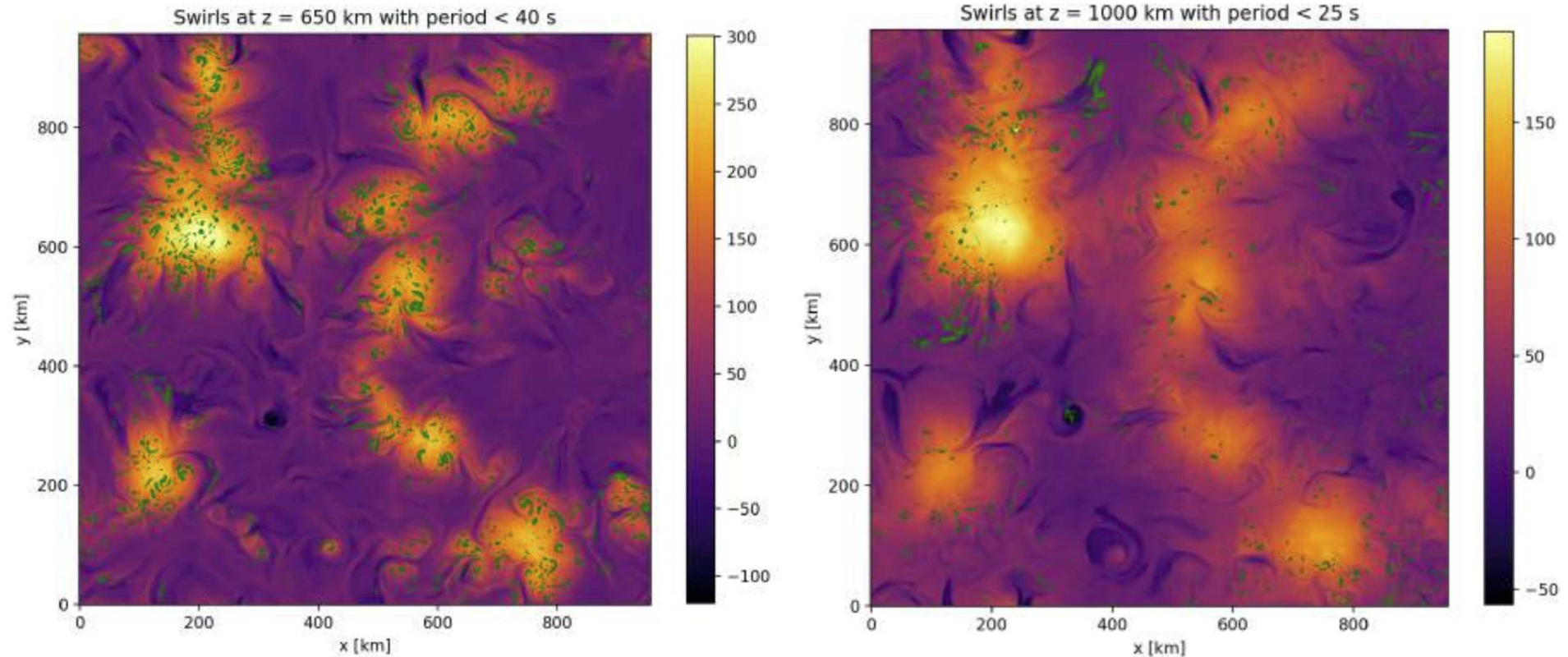
Indentations in magnetic flux concentrations: a source of swirls?



B_z 100 km below $\tau=1$ (background). Vertically directed swirls at same height (blue) and 50 km higher up (green) and overlaps (red). From *Bossart, A., 2018*.

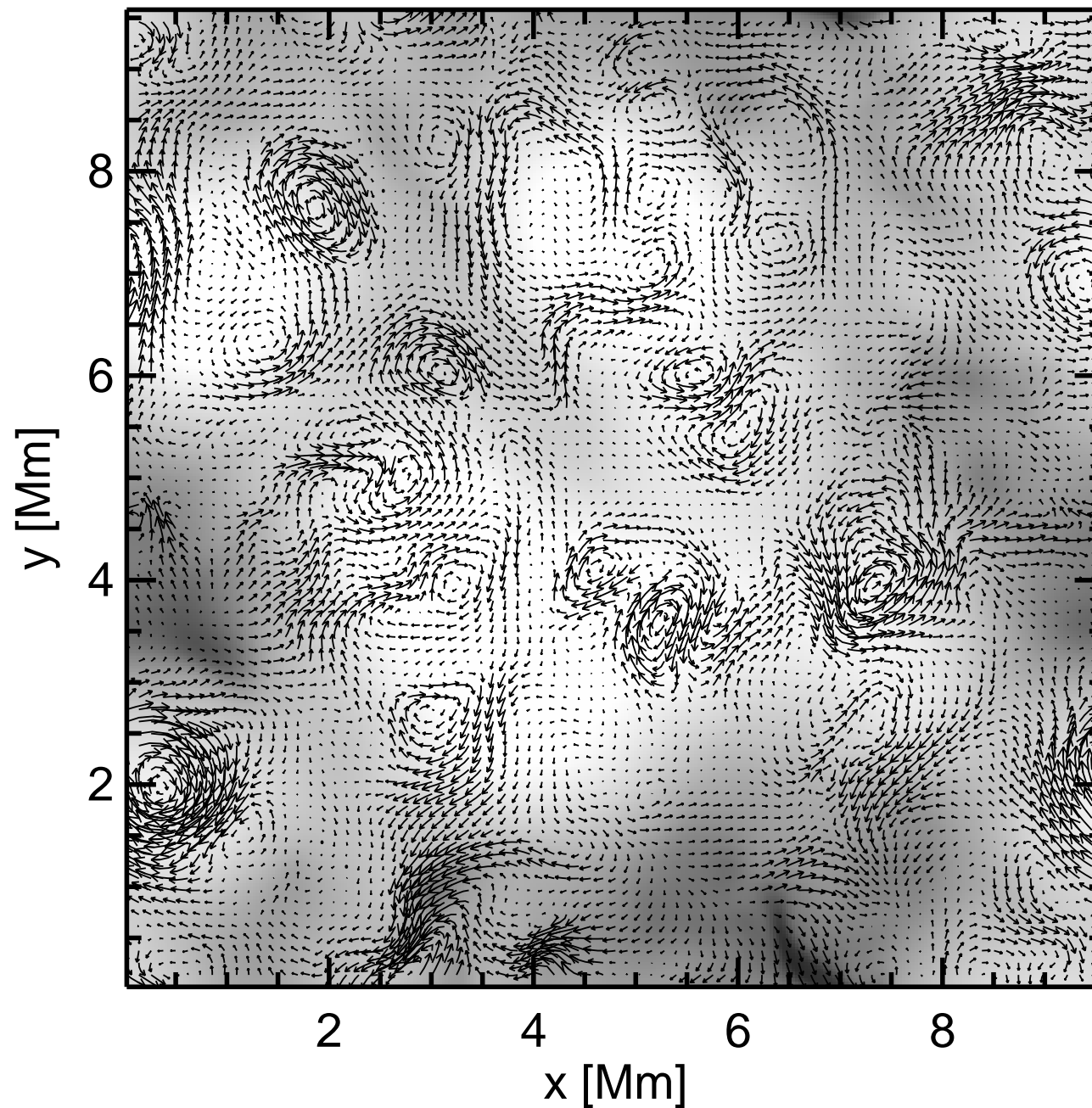
Interaction of a magnetic flux element (red) with convective flows (blue) resulting in a distortion of the flux tube and generation of transverse motions inside it (green arrows), which create Alfvén waves that propagate into the upper atmosphere. From *van Ballegooijen et al. 2011, ApJ 736:3*.

§ 3 Swirls in the solar atmosphere (cont.)



Swirling strength (green) over magnetic field strength (reddish) in the photosphere (left) and the chromosphere (right).

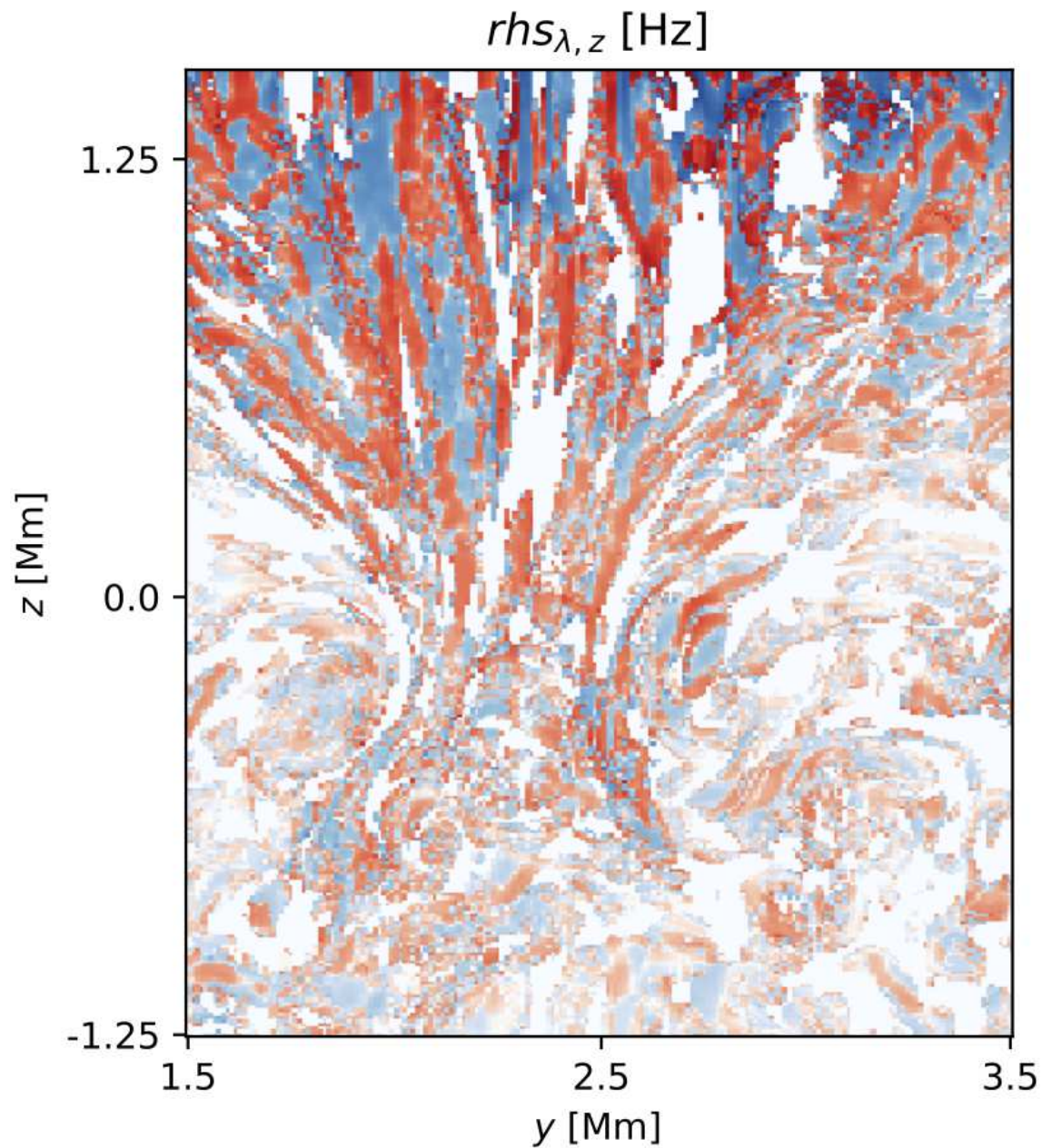
§ 3 Swirls in the solar atmosphere (cont.)



Time instant of the velocity field projected into the horizontal plane at 1300 km above $\langle \tau_c \rangle = 1$. Overplotted in gray scale is $\log |B|$ from 1 to 100 G.

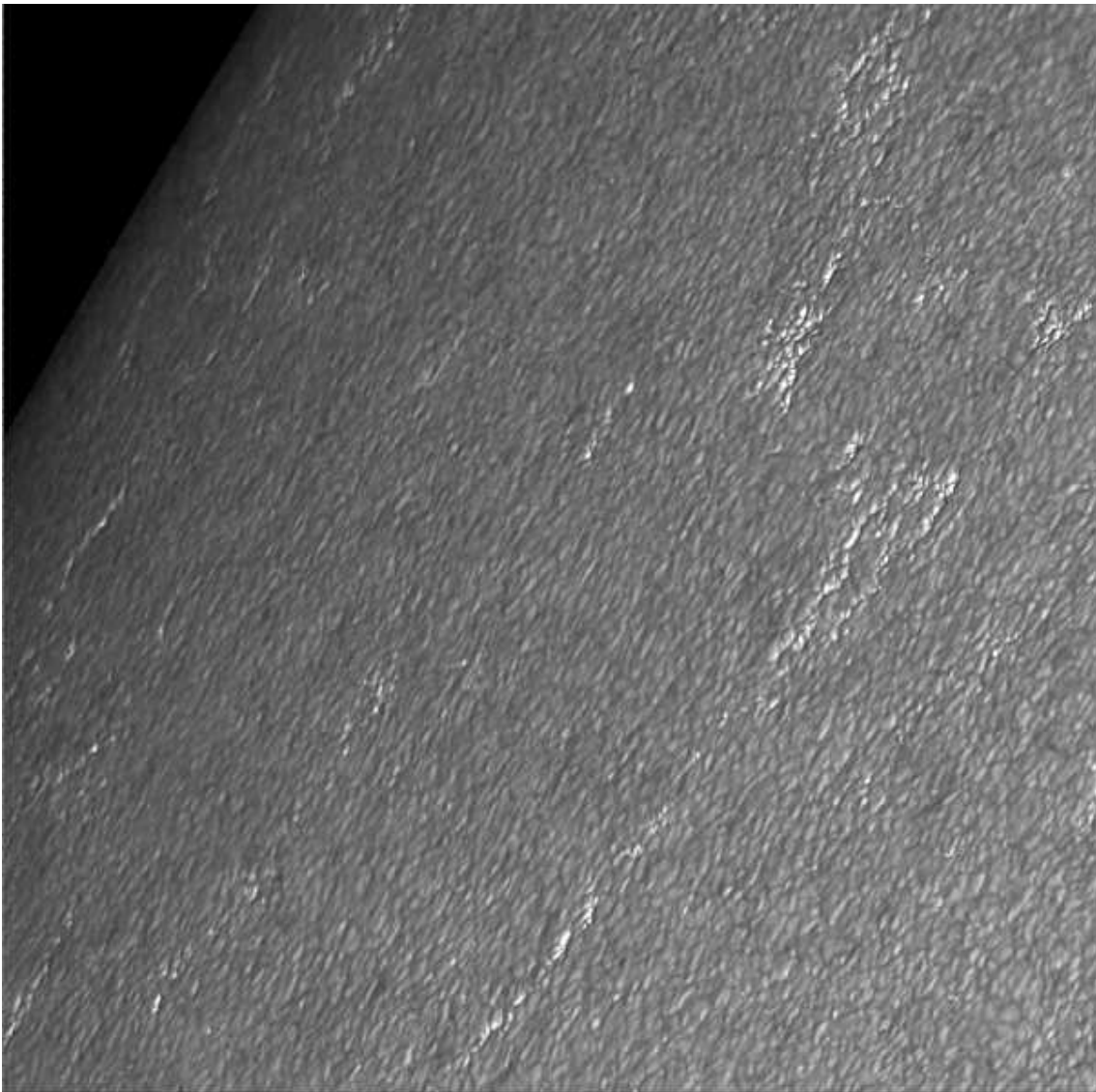
Snapshot from simulation v50, which started with a homogeneous, vertical magnetic field of 50 G. From *Steiner & Rezaei, 2012*.

§ 3 Swirls in the solar atmosphere (cont.)



Patchy appearance of the rate of the vertical and magnetic component of the swirling strength hints at considerable substructure of swirls within magnetic flux concentrations. From *Canivete Cuissa, J.-R., 2019, IRSOL internal report.*

§ 4 Discovering MHD fine structure of faculae with DKIST



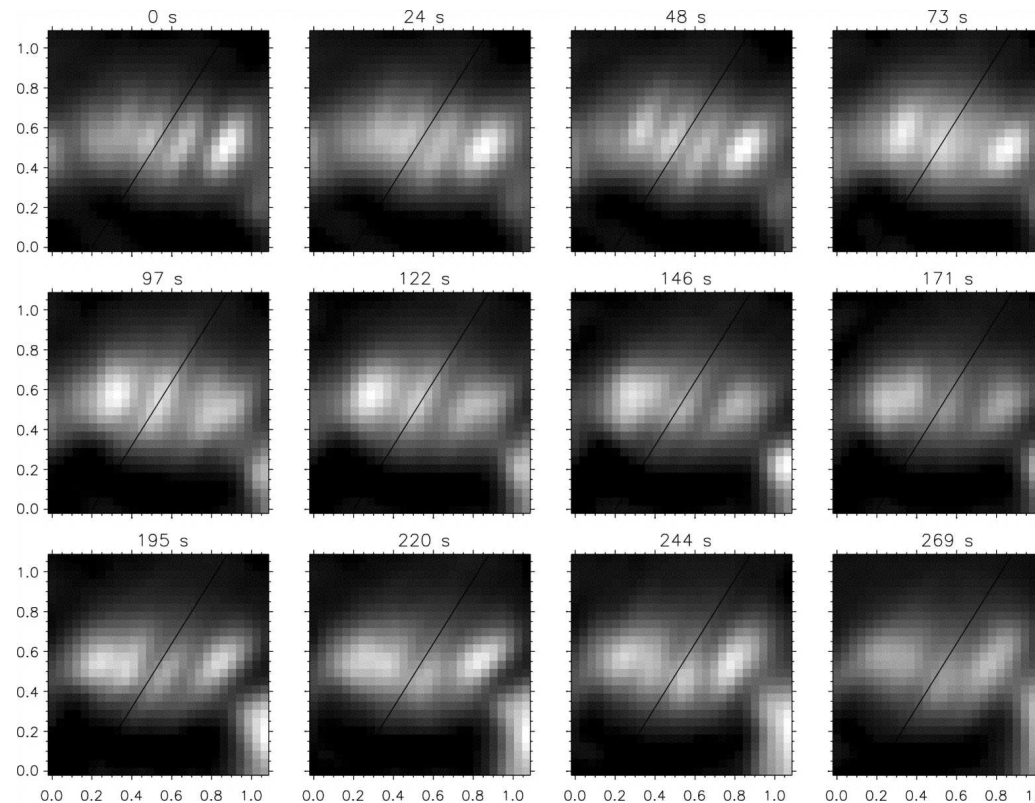
Speckle reconstructed
image of facular region
taken with the 1 m Swedish
Solar Telescope in the
continuum at 487.5 nm.
Field of view approximately
 $80'' \times 80''$.

*From Hirzberger & Wiehr
(2005), A&A 438, 1059*

§ 4 Discovering MHD fine structure of faculae with DKIST (cont.)

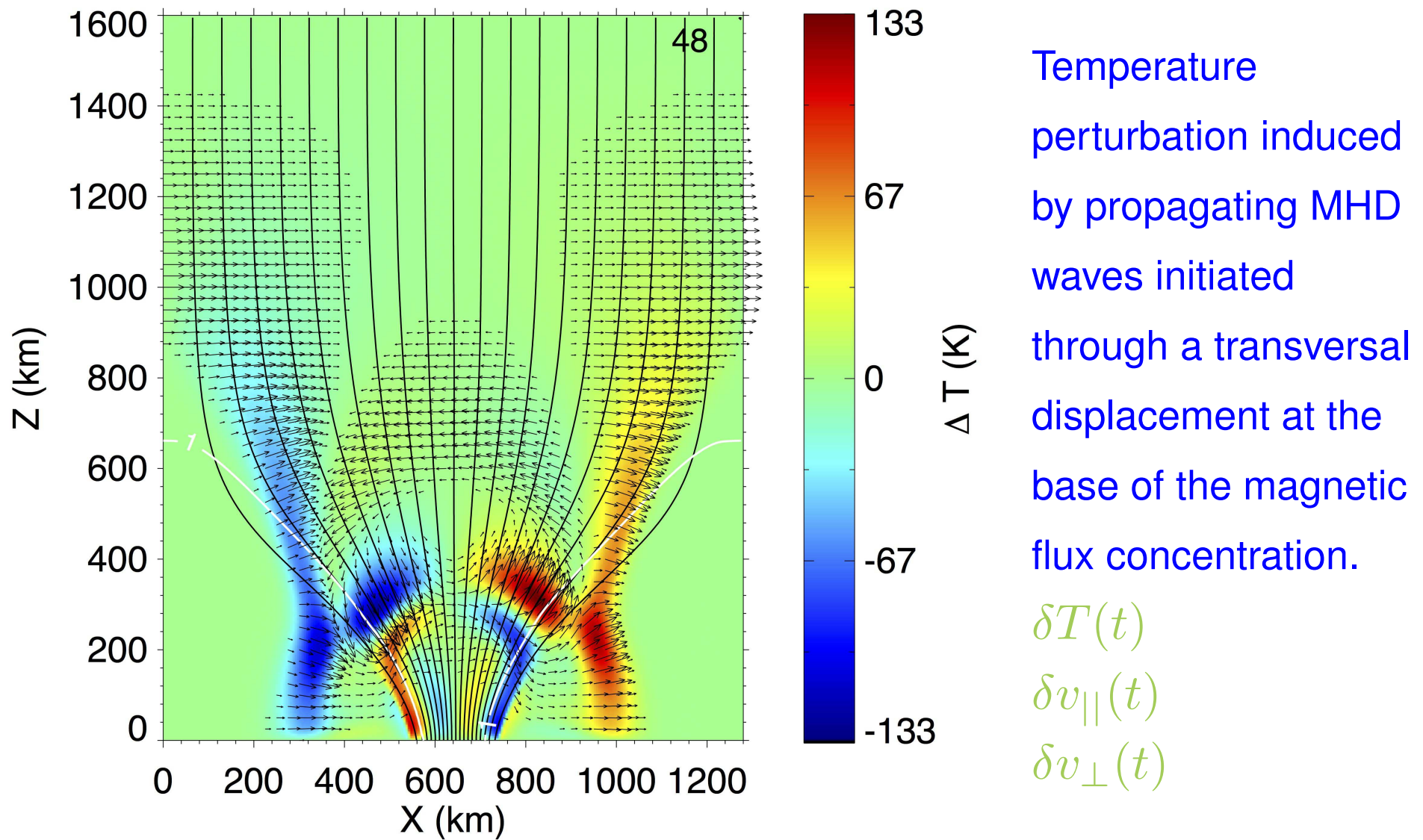
Temporal variability of facular magnetic field. Swaying flux tube?

De Pontieu et al. (2006), ApJ 646, 1405



Faulae provide us with the unique opportunity to see footpoints of fluxtubes from the side!

§ 4 Discovering MHD fine structure of faculae with DKIST (cont.)



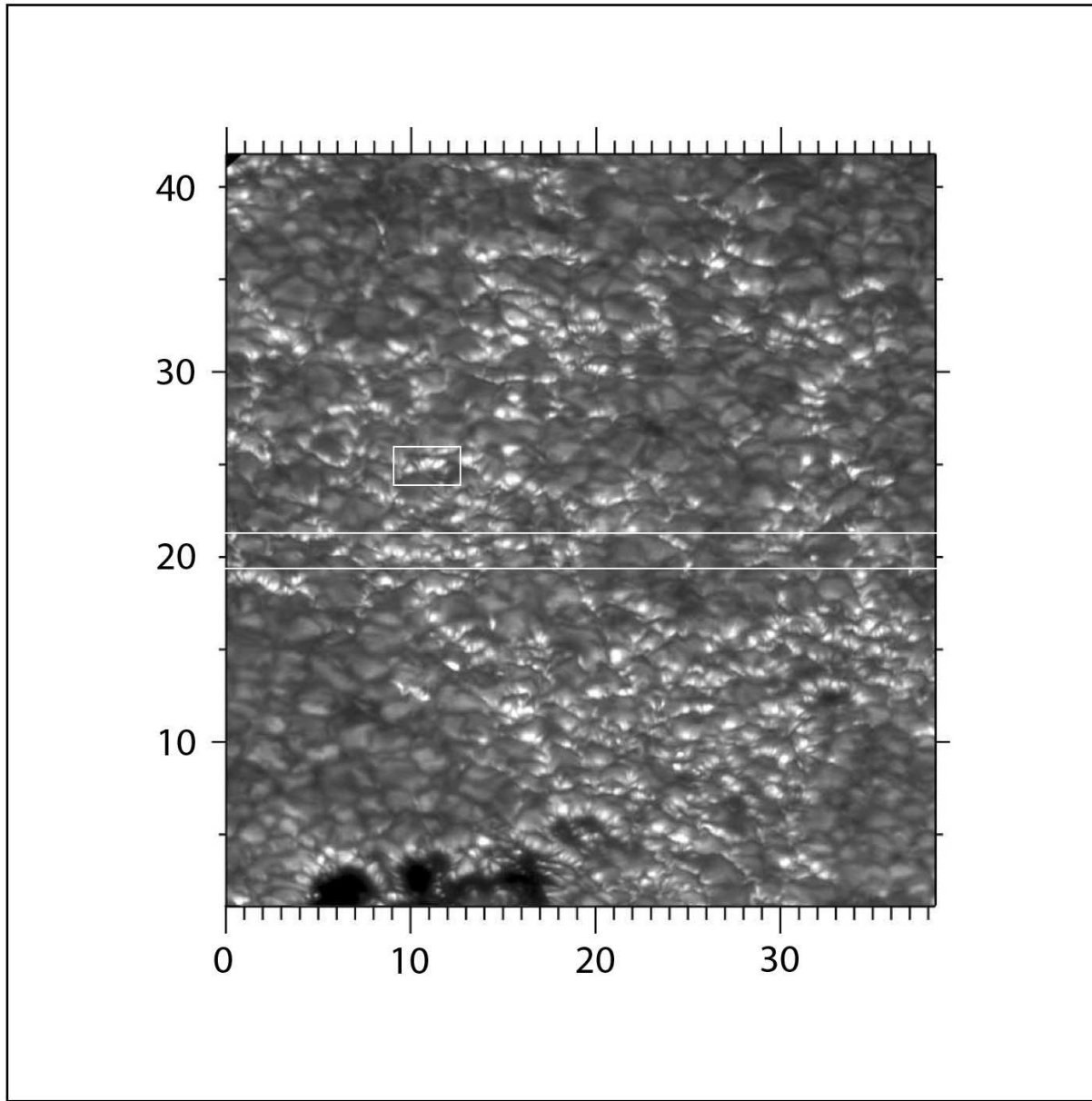
From Vigeesh, Hasan & Steiner: 2009, A&A 508, 951

§ 4.1 Instrument set-up

Instrument	FOV	channel	λ [nm]	cadence	sensitivity	comment
VBI	$45'' \times 45''$	G-band	430.52	3.2 s	S/N = 209	$S/N = 209 \hat{=} \delta T = 10\text{ K}$
VTF	$60'' \times 60''$	Fe I	630.25	21 s	$P/I = 10^{-3}$	6 accumulations, 2 x 2 binning, 11
						scan steps, $\Delta\lambda = 3.15\text{ pm}$
ViSP	$2'' \times 75''$	Ca II	854.21	1.87 s	S/N = 178	intensity alone, 1 accumulation,
						11 scan steps, $\Delta\lambda = 10.68\text{ pm}$, 5 fast scans after every 21 s
NIRSP	$2.4'' \times 1.8''$	Fe I	525.02 524.71	2.5 min	$P/I = 10^{-3}$	38 slit positions, $\Delta x = 0.053''$,
						slit width $0.053''$, $t_{\text{exp}} = 3.8\text{ s}$
NIRSP			1565	5 s	$P/I = 5 \cdot 10^{-3}$	$\delta B = 100\text{ G}$ detectable

Foresee to sequentially observe 5 facular targets at $\mu \approx 0.6$, each for 20 min.

§ 4.1 Instrument set-up (cont.)



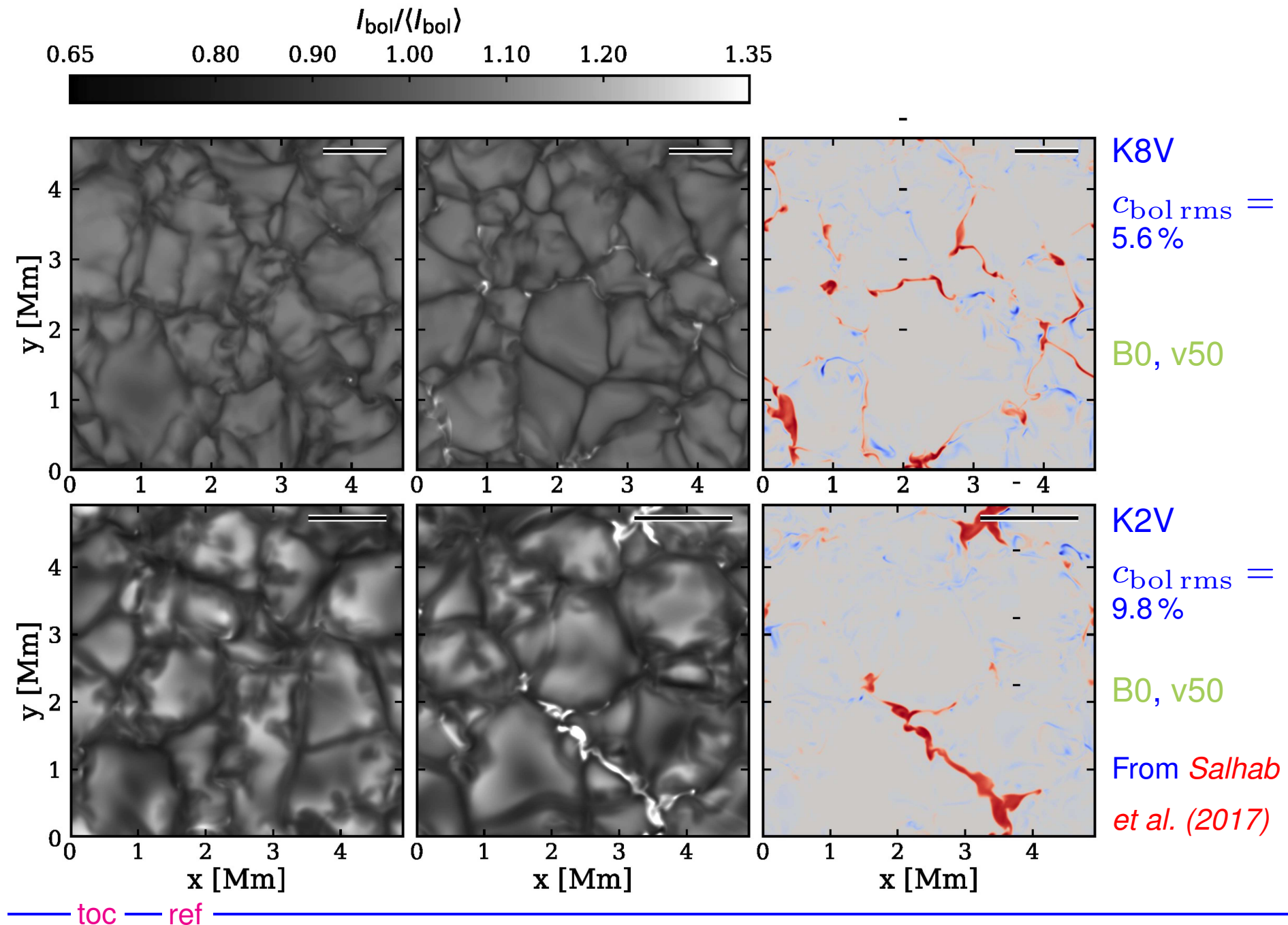
Field of views of VTF
(outermost black frame),
VBI (approximately image
size), ViSP scan area
(white slit across image),
and DL-NIRSP (white
small frame).

§ 5 Current CO5BOLD models at KIS and IRSOL

At KIS, we run five different *stellar atmospheric models*, each once with an initial homogeneous vertical magnetic field of a flux density of 50 G and once without magnetic field but with the same HLLMHD solver.

model name	T_{eff}	$\log g$	B_z^{init}	$X \times Y \times Z [\text{km}^3]$	$\Delta_{x,y}$	Δ_z	$N_x \times N_y \times N_z$	$t [\text{h}]$
d3t33g45rs	3300	4.5	0	$2394 \times 2394 \times 1629$	4.5	4.5	$532 \times 532 \times 362$	5.6
d3t33g45v50rs	"	"	50	"	"	"	"	2.5
d3t40g45rs	4000	4.5	0	$4734 \times 4734 \times 1232$	9.0	7.0	$526 \times 526 \times 176$	10.5
d3t40g45v50rs	"	"	50	"	"	"	"	10.5
d3t40g45v100rs	"	"	100	"	"	"	"	10.5
d3t50g45rs	5000	4.5	0	$4928 \times 4928 \times 2484$	11.0	9.0	$448 \times 448 \times 276$	10.5
d3t50g45v50rs	"	"	50	"	"	"	"	10.5
d3t50g45v100rs	"	"	100	"	"	"	"	10.5
d3gt57g44rs	5770	4.44	0	$5600 \times 5600 \times 2256$	14.0	12.0	$400 \times 400 \times 188$	10.5
d3gt57g44v50rs	"	"	50	"	"	"	"	10.5
d3gt57g44v100rs	"	"	100	"	"	"	"	10.5
d3t65g45rs	6500	4.5	0	$8388 \times 8388 \times 4020$	18.0	15.0	$466 \times 466 \times 268$	10.5
d3t65g45v50rs	"	"	50	"	"	"	"	10.5
d3t65g45v100rs	"	"	100	"	"	"	"	10.5

§5 Current CO5BOLD models at KIS and IRSOL (cont.)

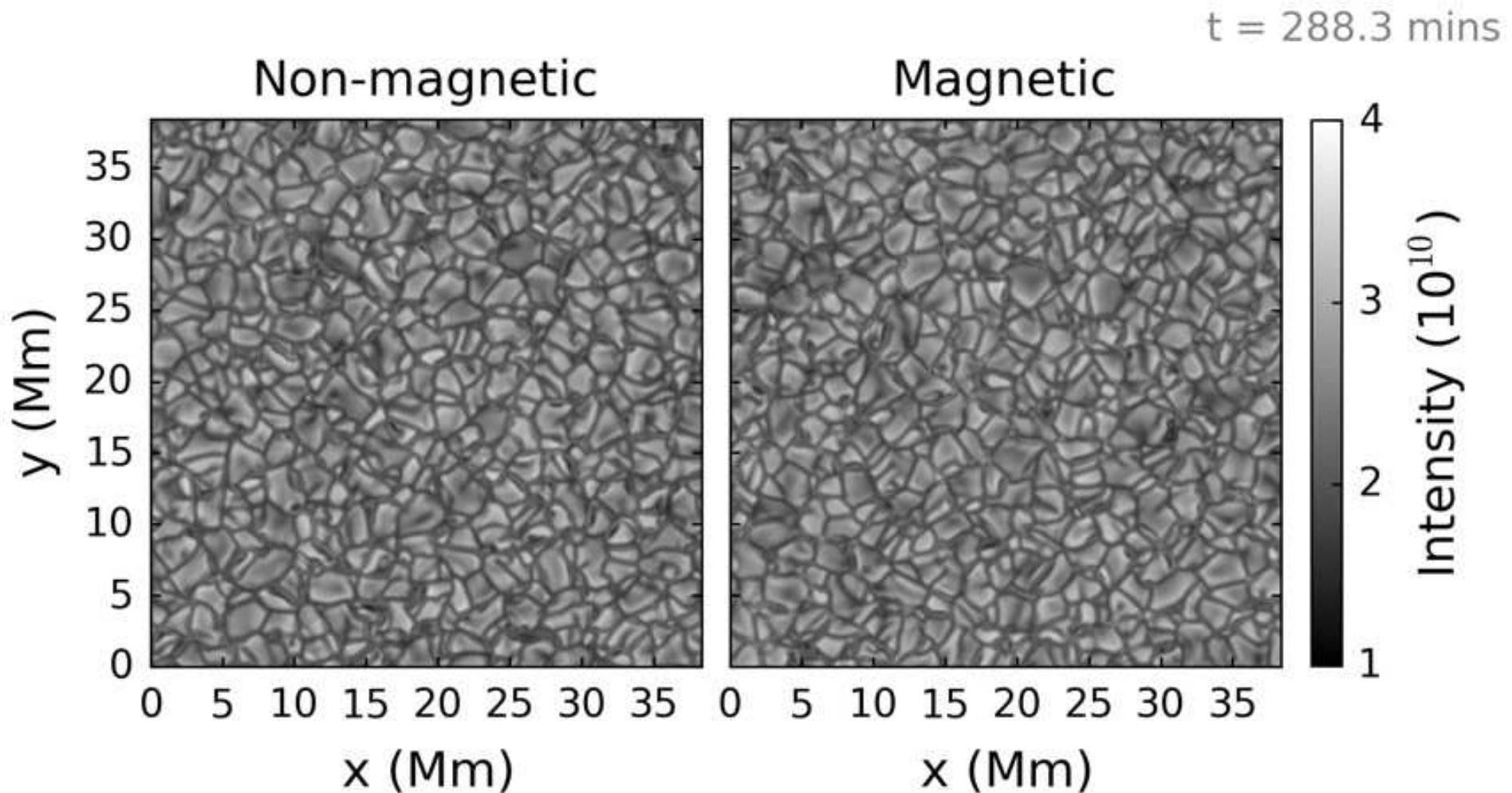


2. Current CO5BOLD models at KIS and IRSOL (cont.)

Also at KIS, G. Vigeesh is running a model of large surface area of $38.4 \times 38.4 \text{ Mm}^2$, with and without magnetic field.

model name	T_{eff}	$\log g$	B_z^{init}	$X \times Y \times Z [\text{km}^3]$	$\Delta_{x,y}$	Δ_z	$N_x \times N_y \times N_z$	$t [\text{h}]$
d3t57g45gv	5770	4.44	0	$38400 \times 38400 \times 2800$	80	20–50	$480 \times 480 \times 120$	8.0
d3t57g45v10gv	"	"	10	"	"	"	"	8.0
d3t57g45v50gv	"	"	50	"	"	"	"	8.0
d3t57g45v100gv	"	"	100	"	"	"	"	8.0

2. Current CO5BOLD models at KIS and IRSOL (cont.)



Vigeesh uses these models for studying *gravity waves*, in particular the differences in the propagation of gravity waves between the magnetic and the non-magnetic model.

2. Current CO5BOLD models at KIS and IRSOL (cont.)

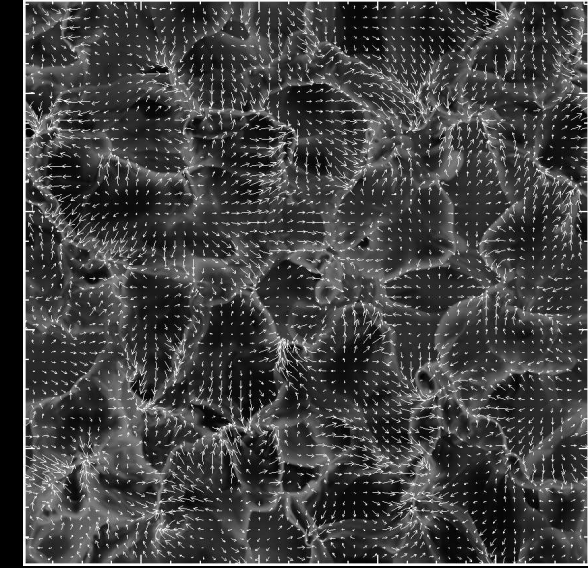
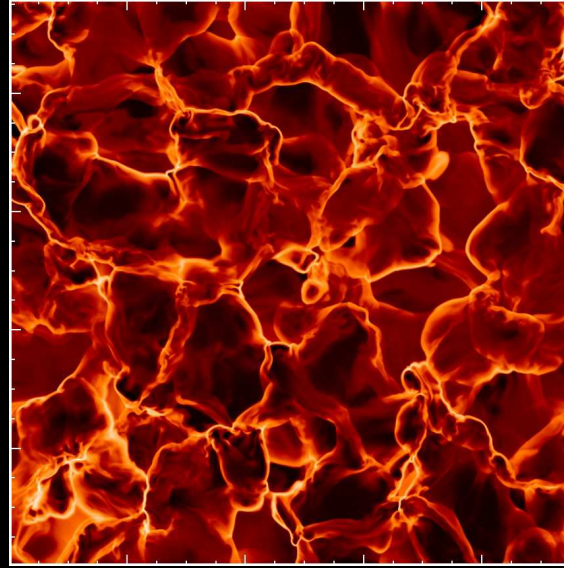
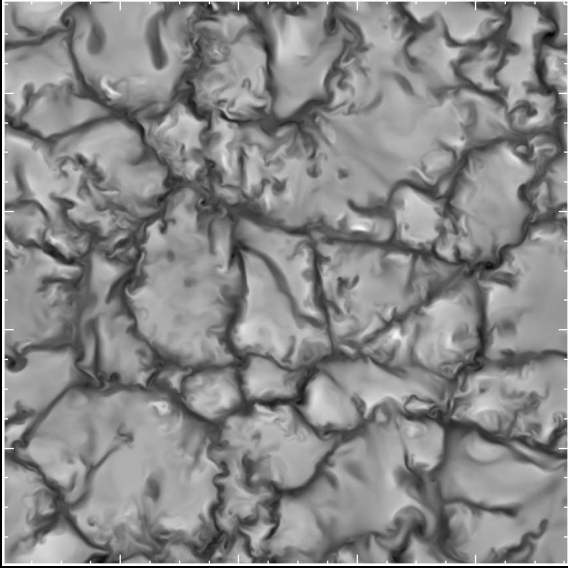
At IRSOL, Flavio Calvo is running high resolution solar models (grid size 10 km) with and without magnetic field and various initial field configurations.

model name	T_{eff}	$\log g$	$X \times Y \times Z [\text{km}^3]$	$\Delta_{x,y}$	Δ_z	$N_x \times N_y \times N_z$	$t [\text{h}]$
d3t57g45fc	5770	4.44	$9600 \times 9600 \times 2800$	10	10	$960 \times 960 \times 280$	2.0

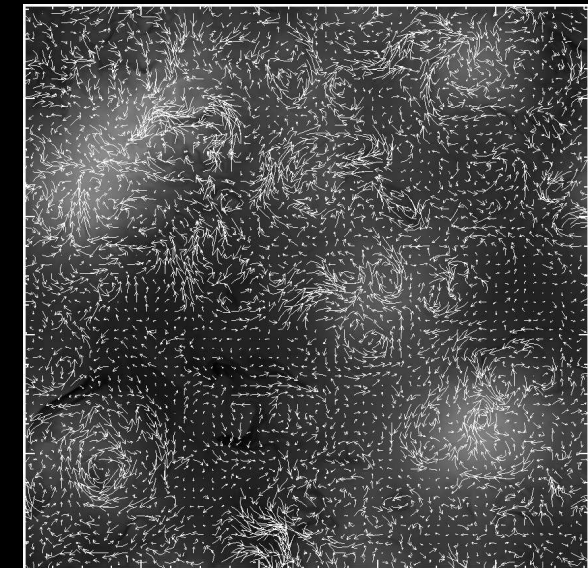
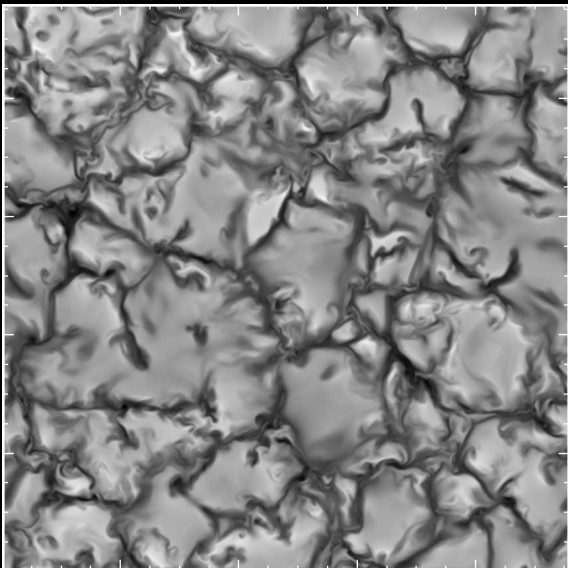
model name	solver	initial magnetic field configuration	$t [\text{h}]$
d3t57g45b0roefc	Roe	no magnetic field	2.0
d3t57g45b0fc	HLLMHD	no magnetic field	2.0
d3t57g45v50fc	HLLMHD	vertical, homogeneous, 50 G	2.0
d3t57g45v200fc	HLLMHD	vertical, homogeneous, 200 G	2.0
d3t57g45v50fc	HLLMHD	horizontally inflowing, 50 G	2.0
d3t57g45p200fc	HLLMHD	potential filed configuration	2.0

He uses these models for *i)* statistical properties of “*non-magnetic bright points*”, *ii)* a study of *Stokes-V line ratios*, and *iii)* for the computation of the center-to-limb variation of the *continuum polarization*.

Solar model, magnetic field-free, 9.6 x 9.6 Mm



Solar model, initial homogeneous vertical 50 G magnetic field, 9.6 x 9.6 Mm



v_z at $\langle \tau \rangle = 1 = z = 0$

T ($z=1200$ km)

v_{hor} ($z=1200$ km)

Piz Daint @ CSCS in Lugano



Piz Daint is a Cray XC50/XC40 with nodes of 12 cores with 64GB RAM and nodes with 18 cores and 128GB RAM, both Intel® Xeon® E5.

Table of content

§ 1 Wave conversion: a numerical experiment

 § 1.1 Magnetic halos and shadows

§ 2 Gravity waves

§ 3 Swirls in the solar atmosphere

§ 4 Discovering MHD fine structure of faculae with DKIST

 § 4.1 Instrument set-up

§ 5 Current CO5BOLD models at KIS and IRSOL

References

References

- Bossart, A.: 2018, *Chromospheric Swirls and Sub-photospheric Flux Tubes*, IRSOL internal report
- Canivete Cuissa, J.-R.: 2019, *Vortices detection and evolution in solar simulations: a dynamical equation for the swirling strength*, IRSOL internal report
- De Pontieu, B., Carlsson, M., Stein, R., Rouppe van der Voort, L., Löfdahl, M., van Noort, M., Nordlund, Å., & Scharmer, G.: 2006, *Rapid Temporal Variability of Faculae: High-Resolution Observations and Modeling*, ApJ, 646, 1405-1420
- Hirzberger, J. and Wiehr, E.: 2005, *Solar limb faculae*, , Astron. Astrophys. **438**, 1059-1065
- Komm, R., De Moortel, I., Fan, Y., Ilonidis, S. and Steiner, O.: 2015, *Sub-photosphere to Solar Atmosphere Connection*, in Helioseismology and Dynamics of the Solar Interior, J. Len Culhane et al. (eds.), Space Science Reviews 196, 167-199
- Newington, M.E. and Cally, P.S. 2010, MNRAS, 402, 386
- Nutto, C., Steiner, O., & Roth, M.: 2012, *Revealing the nature of magnetic shadows with numerical 3D-MHD simulations*, A&A, 542, L30
- Nutto, C., Steiner, O., Schaffenberger, W., & Roth, M.: 2012, *Modification of wave propagation and wave travel-time by the presence of magnetic fields in the solar network atmosphere*, A&A 538, A79

- Salhab, R.G., Steiner, O., Berdyugina, S.V., Freytag, B., Rajaguru, S. P., and Steffen, M.: 2017, *Simulation of the small-scale magnetism in main sequence stellar atmospheres*, Astron. & Astrophys. 614, A78
- Steiner, O., Calvo, F., Salhab, R.G., and Vigeesh, G.: 2017, *CO5BOLD for MHD: progresses and deficiencies*, Mem. Soc. Astr. Ital. 88, 37
- Steiner, O. & Rezaei, R.: 2012, *Recent Advances in the Exploration of the Small-Scale Structure of the Quiet Solar Atmosphere: Vortex Flows, the Horizontal Magnetic Field, and the Stokes-V Line-Ratio Method*, in L. Golub, I. De Moortel, and T. Shimizu (eds.), Hinode 5: Exploring the Active Sun, ASP Conf. Ser. 456, p. 3-32.
- van Ballegooijen, A. A., Asgari-Targhi, M., Cranmer, S. R., and DeLuca, E. E.: 2011, *Heating of the Solar Chromosphere and Corona by Alfvén Wave Turbulence*, ApJ 736, 3
- Vecchio, A., Cauzzi, G., Reardon, K. P., Janssen, K., & Rimmele, T.: 2007, *Solar atmospheric oscillations and the chromospheric magnetic topology*, A&A 461, L1
- Vigeesh, G., Hasan, S.S., and Steiner, O.: 2009, *Wave propagation and energy transport in the magnetic network of the Sun*, A&A 508, 951-962
- Vigeesh, G., Jackiewicz, J., and Steiner, O.: 2016, *Internal gravity waves in the magnetized solar atmosphere: I. Magnetic field effects*, ApJ 835, 148

- Vigeesh, G., Roth, M., Steiner, O., and Jackiewicz, J.: 2019, *Internal gravity waves in the magnetized solar atmosphere: II. Energy transport*, ApJ 872, 166
- Zhou, J., Adrian, R.J., Balachandar, S., and Kendall, T.M.: 1999, *Mechanisms for generating coherent packets of hairpin vortices in channel flow*, J. Fluid Mech. 387, 353